ARTICLE   OPEN

The impact of Atlantic Multidecadal Variability on Baltic Sea temperatures limited to winter

Florian Börgel [1 ✉], Matthias Gröger[1], H. E. Markus Meier[1,2], Cyril Dutheil [1], Hagen Radtke[1] and Leonard Borchert [3]

We analyze multidecadal temperature fluctuations of the Atlantic Ocean and their influence on Northern Europe, focusing on the Baltic Sea, without a priori assuming a linear relationship of this teleconnection. Instead, we use the method of low-frequency component analysis to identify modes of multidecadal variability in the Baltic Sea temperature signal and relate this signal to the Atlantic climate variability. Disentangling the seasonal impact reveals that a large fraction of the variability in Baltic Sea winter temperatures is related to multidecadal temperature fluctuations in the North Atlantic, known as Atlantic Multidecadal Variability (AMV). The strong winter response can be linked to the interaction between the North Atlantic Oscillation and the AMV and is maintained by oceanic inertia. In contrast, the AMV does not influence the Baltic Sea's summer and spring water temperatures.

INTRODUCTION

Subject to non-linear processes, the climate system often shows quasi-non-deterministic behavior[1]. Therefore, detecting the influence of multidecadal signals in regional climate systems is challenging and essential to estimate their interaction with global climate change on multidecadal to multi-centennial time scales. This work investigates the influence of multidecadal sea surface temperature (SST) fluctuations in the North Atlantic Ocean (the so-called Atlantic Multidecadal Variability or AMV for short[2]) on Northern European temperature, focusing on the Baltic Sea.

During the 20th century, the North Atlantic changed between anomalous warm and cold SST on multidecadal time scales. The main driver of these fluctuations, which are summarized as the AMV, is still heavily debated, but its origin is likely a combination of internal variability and response to external forcing[3–5]. Both observational and modeling studies agree that AMV influences the climate in Europe[6]. The AMV has been linked to altered temperature and precipitation patterns across Europe[6–9]. It strongly impacts summer temperatures in western and central Europe[3]. During the negative AMV phase in the 1960s–1990s, summers were cooler across large parts of Europe, whereas the recent positive phase resulted in warmer springs, summers, and autumns in Northern Europe[3,6,10].

During winter, the NAO is the most prominent mode of climate variability in the North Atlantic sector[11]. In winter, it is responsible for more than 80% of the sea level pressure (SLP) variability over the North Atlantic and Europe[12]. Recent studies argue for a dynamic coupling between the NAO and the AMV[7–9,13–15]. Strong zonal winds over the North Atlantic (likely associated with positive NAO anomalies) lead to anomalous heat loss in the Labrador Sea, enhancing deep-water formation and strengthening the Atlantic meridional overturning circulation (AMOC). Stronger AMOC-driven poleward heat transport helps to compensate for the initial cooling, leading to basin-wide warming on multidecadal time scales. The atmosphere then adjusts to the Atlantic warming. The years following the AMV maximum are characterized by negative NAO conditions, a weakening AMOC, and, consequently, colder SSTs over the Atlantic which in turn feed back onto AMV, North

Atlantic temperatures, and the AMOC[3,7,9,16,17]. Hence, the AMOC and the AMV are influenced by the time-integrated effect of the NAO. At the same time, the resulting ocean response likely affects the NAO[9].

Traditionally, the AMV signal and the associated multidecadal variability within the North Atlantic basin were analyzed by spatially averaging SST anomalies north of the equator (0°–60°N, 0°–80°W). Trenberth and Shea[2] proposed to remove the global SST signal instead of linear detrending[18], which allows isolating variability within the North Atlantic. While the estimation of the amplitude and phase of the AMV are sensitive to the detrending method[19], the method proposed by Trenberth and Shea[2] has been proven suitable for analyzing multidecadal variability. It may cause an underestimation of the variability in the North Atlantic, but it also removes the impact of global warming[20]. However, Wills et al.[14] argued that the choice of the averaging region is problematic, as no physical mechanism has been proposed that is limited to the area between the equator and 60°N. To avoid any a priori assumption about the spatial and temporal structure, Wills et al.[14] developed a method called low-frequency component analysis (LFCA), which allows for finding spatial anomaly patterns with the highest ratio of low frequency to the total variance. Using LFCA, they disentangled influences of high-frequency variability, multidecadal variability, and long-term global warming.

While the AMV's impact on long-term land climate has been investigated[6,10,21], its effects on coastal regions and large water bodies of marginal seas have not yet been studied in detail. The Baltic Sea has limited water exchange with the North Atlantic, and its variability is mainly controlled by atmospheric forcing. Its large water body (21,500 km³) filters high-frequency temperature fluctuations and is therefore well-suited to study long-term atmospheric teleconnections.

Börgel et al.[22] found that the Baltic Sea, like many other regional climate systems, is influenced by the AMV. They estimated that multidecadal salinity changes of 1 g/kg—about 10% of the Baltic Sea's mean salinity—could be linked to the AMV. Moreover, SST and sea ice cover were also found to be influenced by the AMV.

[1]Leibniz Institute for Baltic Sea Research Warnemünde, Rostock, Germany. [2]Swedish Meteorological and Hydrological Institute, Norrköping, Sweden. [3]Center for Earth System Research and Sustainability CEN, Universität Hamburg, Hamburg, Germany. ✉email: florian.boergel@io-warnemuende.de
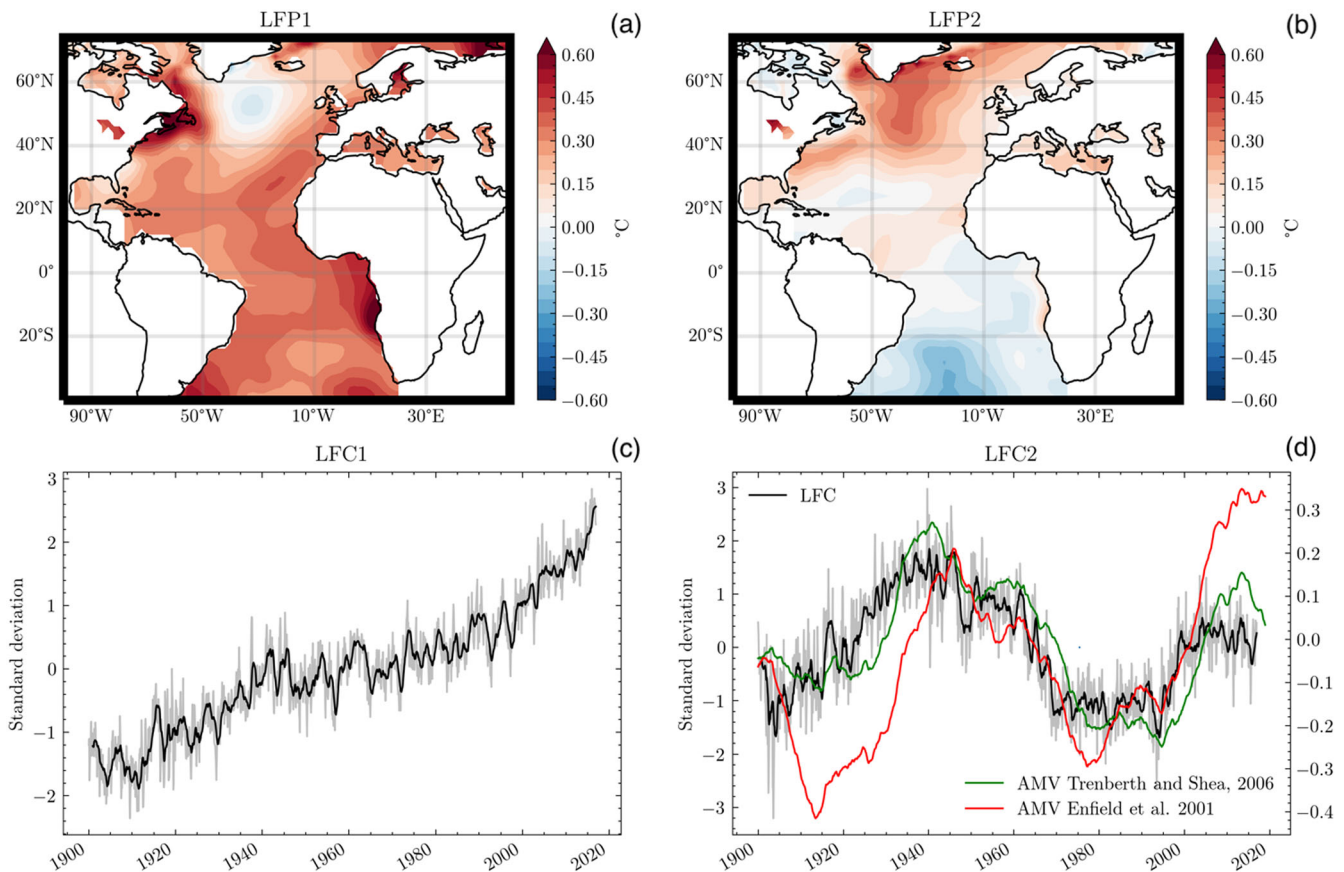
Fig. 1 **Low-frequency component analysis of the Atlantic sea surface temperature (SST) anomalies from ERSST.** The first and second low-frequency patterns (**a**, **b**) (LFP) and low-frequency components (**c**, **d**) (LFC) retaining 30 EOFs and a 10-y low-pass cutoff are shown. LFC1 (global warming in the Atlantic) shows a 1-y running mean in black, whereas the gray line shows monthly fluctuations. LFC2 (Atlantic Multidecadal Variability, AMV) shows a 1-y running mean in black and monthly changes in gray. The AMV definitions of Enfield et al. (2001) and Trenberth and Shea (2006a) have been added in red and green, respectively.

Kniebusch et al.[17] analyzed the impact of the AMV on the SST in the Baltic Sea and found that 58% of the decadal SST variability of the Baltic Sea could be linked to the AMV when the global warming signal is removed. It is estimated that the AMV's impact on the SST of the Baltic Sea on annual time scales is relatively small, with a 5% explained variance, assuming that winter and annual SST responses to AMV variability are similar[23].

Multiple studies found that a positive AMV is followed by a negative NAO state[3,9,13,15–17], which is likely associated with colder and drier winters in Northern Europe[24]. However, there is no analysis focusing on the seasonality of the AMV and its impact on the temperature in the Baltic Sea region.

Therefore, this study aims to estimate the seasonal impact of the AMV on temperature variability in Northern Europe, specifically the Baltic Sea region. To assess the low-frequency variability, we use LFCA. This method avoids possible inaccuracies[25] since it takes non-linearities into account. This allows us to analyze the dominant low-frequency signals within the Baltic Sea without prior assumptions of linearity, which do not necessarily apply to teleconnections[8].

RESULTS
The AMV
We use LFCA to extract the dominant modes of variability within the North Atlantic SST. We compute the two leading low-frequency components and low-frequency patterns (LFCs and LFPs) of the monthly SST anomalies within the Atlantic basin,

retaining 30 empirical orthogonal functions (EOFs) explaining roughly 90% of the total variance within the North Atlantic (Fig. 1). The first LFP (Fig. 1a) shows a nearly uniform warming pattern and resembles the North Atlantic response to global warming captured by the LFC1 (Fig. 1c)[26]. The second LFP (Fig. 1b) indicates a warming signal north of 0° with a maximum warming pattern in the subpolar gyre, representing the averaging region of the established AMV definition by Trenberth and Shea[2]. The pattern looks like the regression pattern associated with Trenberth and Shea-based AMV index[2]. The corresponding second LFC (Fig. 1d) shows multidecadal temperature fluctuations with a positive period between the 1930s and 1960s, which transitions to a negative phase around 1960 and back into a positive phase in the 1990s. This second LFC shows a high correlation of 0.9 with the established AMV definition of Trenberth and Shea[2] when applying a 10-y running mean. However, compared to the original AMV definition by Enfield et al.[18], it has different amplitudes and phases, suggesting that linear detrending is not capturing the internal component of the North Atlantic variability.

In contrast to the Trenberth and Shea-based AMV index, LFCs are not low-pass filtered and can capture the interaction between high-frequency atmospheric variability and the inertia-driven response of the ocean[14,26]. Hence, in the following, the second LFC can be interpreted as the AMV signal without filtering out processes that operate on shorter time scales than decades.
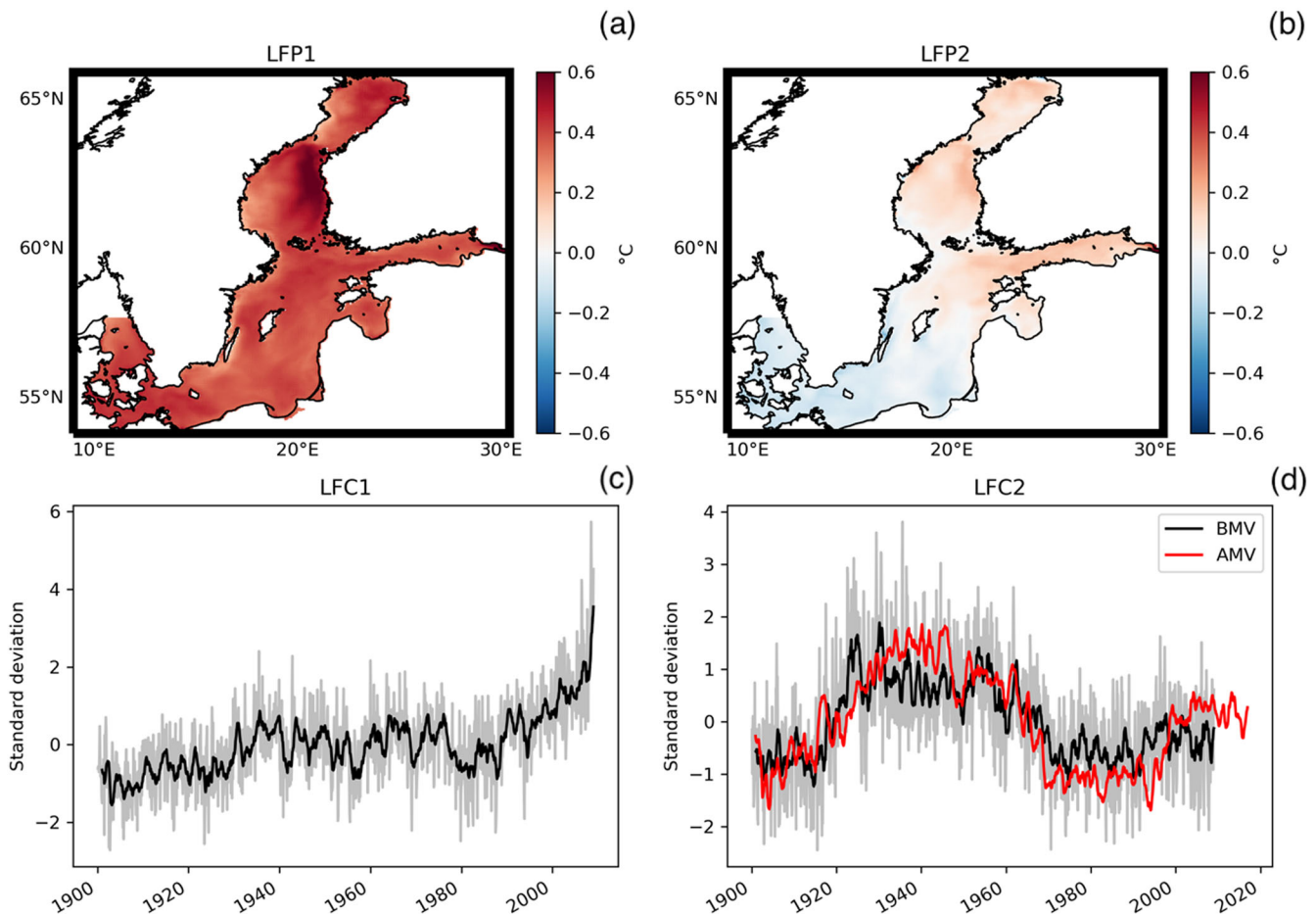
Fig. 2 Low-frequency component analysis of the Baltic Sea sea surface temperature anomalies, extracted from the regional climate model RCO. The first and second low-frequency patterns (**a**, **b**) (LFP) and low-frequency components (**c**, **d**) (LFC) using 200 EOFs retained and a 10-y low-pass cutoff are shown. LFC1 (global warming signal in the Baltic Sea) shows a 1-y running mean in black, whereas the gray line shows monthly fluctuations. LFC2 (Baltic Multidecadal Variability, BMV) shows a 1-y running mean in black and monthly changes in gray. The LFC2 (Atlantic Multidecadal Variability, AMV) computed for the Atlantic Basin (Fig. 1) is shown in red for comparison.

The impact of the AMV on regional climate systems such as the Baltic Sea

The AMV influences the Baltic Sea[22]. Often, when analyzing the response of a regional climate system to climate variability, a linear response is assumed. However, besides the North Atlantic influence, the Baltic Sea is influenced by many other processes with various time scales.

If two assumptions hold, namely that (a) the AMV influences the Baltic Sea and (b) the LFCA proves to be a suitable method to discriminate between different physical forcing mechanisms, it should be possible to disentangle the AMV signal from the total SST variability in the Baltic Sea using LFCA. The second hypothesis (b) is supported by the fact that unlike a time series, e.g., discriminating between frequency bands only, the LFCA method takes spatial information into account and can disentangle processes leaving different spatial footprints. The idea is to distill the AMV-related response within the Baltic Sea, likely influenced by non-linear processes, and therefore get more meaningful results compared to a simple (linear) correlation with the AMV signal.

The Baltic Sea's complex dynamics and the different spatial resolutions of the data products influence the number of EOFs retained. We increased the number of EOFs (N) kept to 200, capturing over 95% of the monthly SST variance. This way, we include variability on smaller spatial scales with significant low-frequency power. This improves isolating patterns of multidecadal

variability and filtering out variability that acts on shorter time scales[26]. We use monthly SST anomalies from the regional ocean model RCO simulating the Baltic Sea for our analysis[27]. The results are robust to changes between $N = 100$ and $N = 250$.

The two dominant LFCs/LFPs that maximize the ratio of low frequency to the total variance in the Baltic Sea are a basin-wide warming response associated with global warming (LFC/LFP1 Fig. 2a, c) and multidecadal temperature fluctuations (LFC/LFP2), shown in Fig. 2. The multidecadal fluctuations of the second LFC (Fig. 2d) project onto a dipole LFP pattern (Fig. 2b), with a warming response in the northeastern part of the Baltic Sea and a cooling reaction within the rest of the Baltic Sea. On an annual timescale, the second LFC of the Baltic Sea SST shows a correlation of 0.72 with the second LFC within the North Atlantic. After applying a 10-y running mean to both signals, we find a correlation of 0.93 between LFC2 in the North Atlantic and the second LFC of the Baltic Sea, indicating the close relationship between both signals. Further, all but the second Baltic LFC show only a small correlation (<0.1) with the North Atlantic LFC2. Even when we consider a possible relationship between the North Atlantic LFC2 and the Baltic LFC1 due to the high amplitude of Baltic LFC1, the results prove robust. This holds independent of the number of LFCs considered.

Still, we decided to use a linear combination of the first two Baltic LFCs and weigh them according to the previously computed correlation coefficients, accounting for the small contribution of
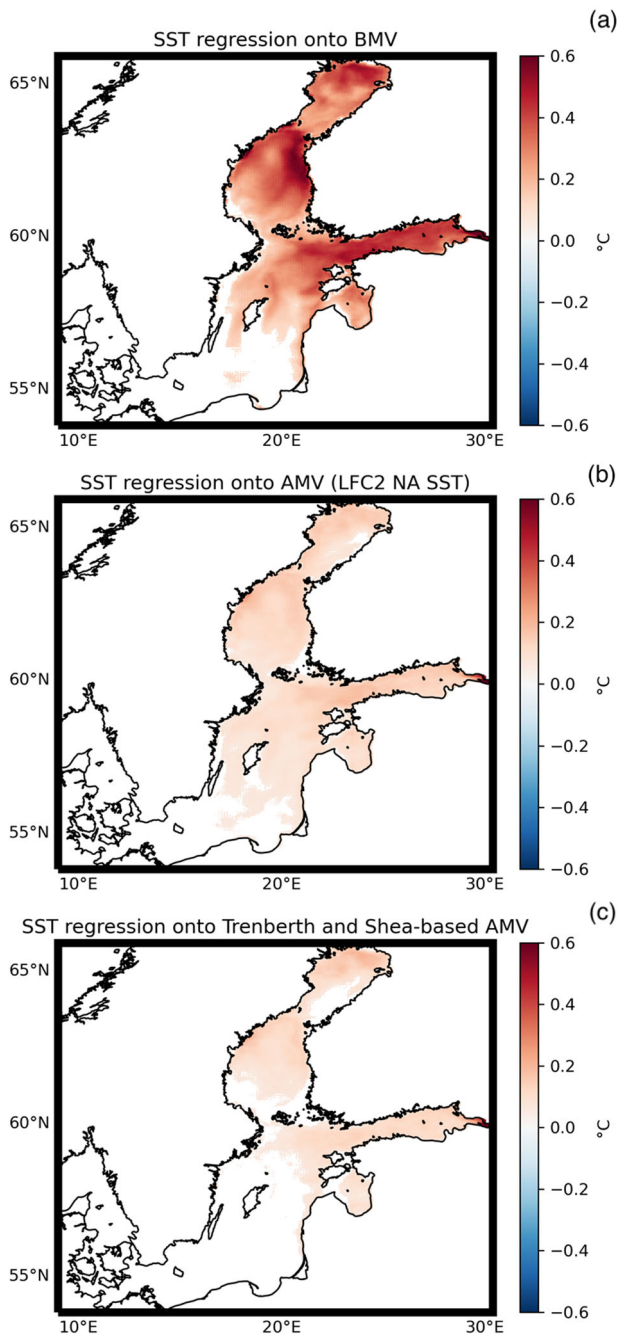
Fig. 3 Baltic Sea sea surface temperature regression patterns using different AMV indices. Linear regression of Baltic Sea sea surface temperature anomalies onto the BMV (**a**) (LFC2 Fig. 2), the AMV (**b**) (LFC2 Fig. 1), and AMV Trenberth and Shea[2] (**c**). Only statistically significant regions ($p < 0.05$) are colored.

the North Atlantic LFC2 to Baltic LFC1. Including the Baltic LFC1 increases the correlation between the North Atlantic LFC2 and the combination of the first two Baltic LFCs on decadal time scales to 0.98. In the following, the resulting signal is defined as Baltic Multidecadal Variability (BMV), and the LFC2 of the Atlantic as AMV.

While the AMV and the BMV are closely coupled on yearly and decadal time scales, on monthly time scales, the correlation drops to 0.55 (not shown). The seasonal cycle was removed from the data. This indicates a close coupling between the AMV and the

BMV in the low-frequency band but a de-coupling of the related intra-annual variability.

Regressing monthly SST anomalies onto the BMV (Fig. 3a), the AMV (NA LFC2) (Fig. 3b), and the traditional Trenberth and Shea-based AMV index (Fig. 3c) results in similar spatial regression patterns. All regression patterns show a uniform warming pattern in the Baltic Sea. However, the AMV and the Trenberth and Shea-based AMV index show a relatively weak amplitude of about 0.2 °C. In contrast, the BMV relates to a strong positive response of up to 0.6 °C, tripling the estimated response by the AMV. Compared to the linear regression based on the Trenberth and Shea-based AMV index, we find that the LFCA-based indices increase the statistically significant area.

The LFCA results in a higher low-frequency to total variance ratio ($r = 0.78$) for the AMV than the BMV, where only about 40% of the signal consists of low-frequency variability (not shown). Accordingly, the AMV signal shows a strong autocorrelation, indicating a higher persistence than the BMV. By contrast, the autocorrelation of the BMV decreases significantly within the first year (not shown). The difference in persistence in the Baltic Sea and the different amplitudes in Fig. 3 suggests that the BMV-related response has a strong seasonality that is not captured by the linear regression of the Baltic Sea SST onto the AMV.

To better understand this seasonal influence, the seasonal SST response associated with the BMV variability is analyzed (Fig. 4). In some regions, up to 40% of the SST variability in winter (Fig. 4a) can be attributed to the BMV, corresponding to temperature fluctuations of 1.2 °C per BMV standard deviation. The most substantial influence is found in the eastern part of the Gulf of Finland, parts of the central Baltic Sea, and the northern Bothnian Sea. These regions share interannual changes in sea ice coverage. During spring (Fig. 4b), there is no significant response. During summer (Fig. 4c), only small regions in the northern part explain more than 5% of the SST variability that can be linked to the BMV for this season. Lastly, the response in autumn (Fig. 4d) shows warming in the northern part of the Baltic Sea and the Gulf of Finland with 10–20% explained variance. The annual mean pattern (Fig. 3) resembles the winter and autumn patterns most strongly, with some summer contributions. We find similar results for the regression patterns of the AMV index (Supplementary Figure 1) and the traditional AMV index by Trenberth and Shea (Supplementary Fig. 2). However, the statistically significant areas are smaller, and there is little to no explained variance.

To analyze the relationship between the AMV, the BMV, and the Baltic Sea during winter, we regress SLP, surface winds (u10, v10), surface air temperature (SAT), and SST onto the AMV and the BMV indices. We consider lags −20 to −5 years, −5 to 5 years, and 5 to 20 years. The regression analysis applies to positive and negative states, but for clarity, the following description is given for a positive event. We find that the regression patterns of the AMV and the BMV are nearly identical (not shown). Therefore, we focus on the response to the AMV (Fig. 5).

For lags −20 to −5 years, we find a negative SLP anomaly over Greenland and Iceland and a positive SLP anomaly south of 50°N in the Atlantic, spanning across Europe (Fig. 5a). The wind regression pattern shows increased westerlies in the subpolar region (40°–60°N, 20°–60°W, Fig. 5b) and increased south-westerlies near Greenland–Iceland–Norwegian (GIN) Seas and the Iceland Basin. While there is an ongoing debate about which high-latitude deep-water formation regions control the AMOC and its variability, the increase in westerlies over the Labrador Sea is associated with enhanced upward turbulent heat fluxes resulting in a lagged strengthening of the AMOC[7,9,16], which enhances poleward heat transport[16]. More recently, the GIN Seas have also been identified as important regions for deep-water formation[28]. Hence, it is likely that the enhanced upward turbulent heat fluxes in the GIN seas also contribute to the stronger deep-water formation, strengthening the AMOC. The SAT response shows a
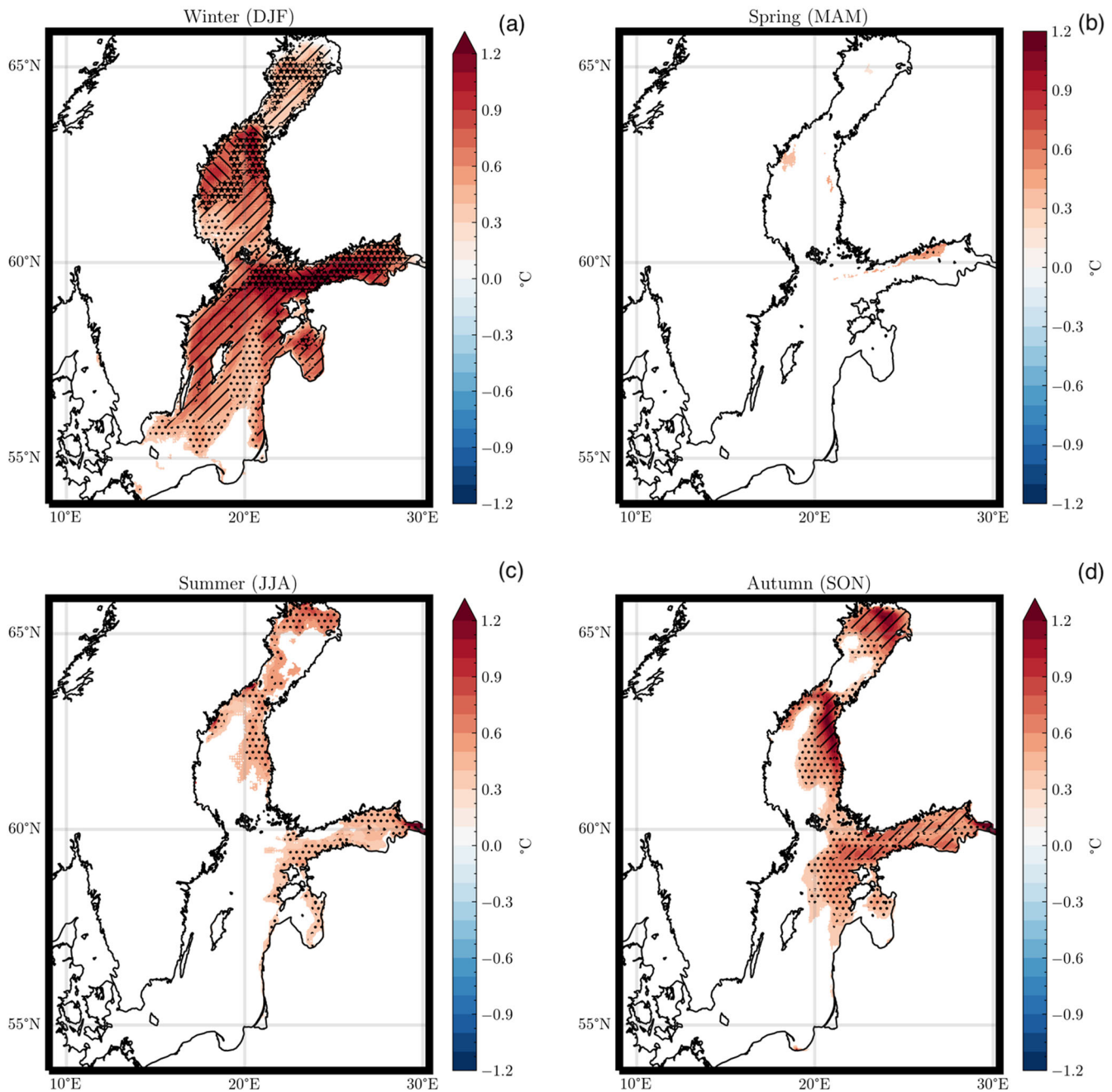
Fig. 4 Seasonal sea surface temperature response associated with BMV variability. Linear regression of seasonal sea surface temperature anomalies onto the seasonal component of the BMV (winter (**a**), spring (**b**), summer (**c**), and autumn (**d**)). The hatching indicates the explained variance. Dots (.) correspond to >5%, side hatching (/) to >10%, stars (*) to >20%, and backward side hatching (\) to >30%, explained variance. Only statistically significant changes are colored ($p < 0.05$; Student's t-test).

near basin-wide warming also reaching the Baltic Sea region (Fig. 5c). In contrast, the SST shows a negative response. At lag −5 to 5 years, the atmosphere shows a weakly negative NAO response in agreement with reduced westerlies and cooling over central Europe. However, the northern part of Europe still shows slightly positive SAT and SST, likely related to the large oceanic inertia and enhanced northward oceanic heat transport. After an AMV maximum at lags 5 to 20 years, stronger negative NAO conditions and a decrease in westerlies likely result in a strong cooling of air temperatures over Europe and the Baltic Sea. In contrast, the larger inertia of the North Atlantic still shows higher SST in the North Atlantic and parts of the Baltic Sea, despite a

cooling effect of the atmosphere. A zoom on the Baltic Sea can be found in the supplementary (Supplementary Fig. 3).

We repeated the same analysis for autumn (Supplementary Fig. 4). During autumn, the atmospheric response is noisier but yields a uniform warming response at lags −20 to 20 around an AMV maximum that also influences the Baltic Sea region.

DISCUSSION
Our study focuses on the emergence of multidecadal fluctuations in regional climate systems. With an LFCA, we have been able to detect multidecadal SST fluctuations in the Baltic Sea (BMV) that
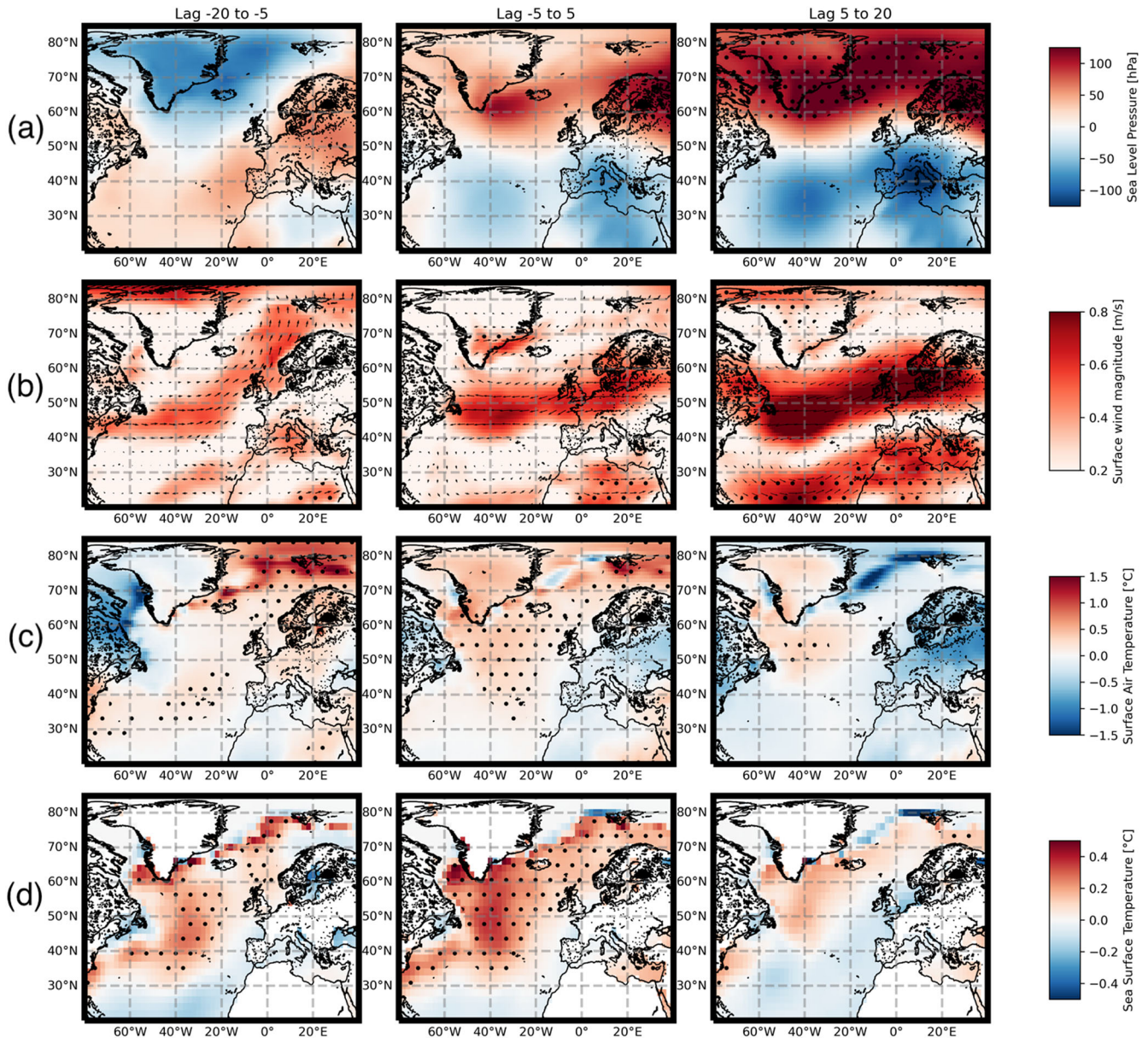
Fig. 5 Regression patterns of ERA20-C associated with AMV variability. Regression of winter sea level pressure (**a**), surface winds (**b**), surface air temperature (**c**), and sea surface temperature onto the AMV (**d**) around an AMV maximum. The left column panel shows lags of −20 to −5 years, the middle column panel shows lags of −5 to 5 years, and the right column panel shows a lag of 5–20 years. The dotted area indicates statistical significance ($p < 0.05$).

bear a strong similarity with the AMV, showing a correlation higher than 0.95 on decadal time scales. We identify the BMV as an important contributor to Baltic Sea SST variability during winter. The impact of the BMV on the Baltic Sea SST variability differs drastically from season to season. While we find a substantial impact of up to 40% explained variance locally during winter, it remains mostly below 5% during spring and summer.

In contrast to other parts of Europe where the AMV also has a substantial impact during summer, for the Baltic Sea, we identify the winter season to be under the strongest influence of the AMV by far. The winter influence is likely caused by the NAO's out-of-phase relationship with the AMV: The impact of the time-integrated NAO forcing on the AMV and AMOC links to basin-wide warming in the North Atlantic (Fig. 5d), which maintains warmer SST despite already weak negative NAO conditions at lag −5 to 5 years. Some studies have already analyzed the AMV's

impact on Northern Europe[22,23]. Ruprich-Robert et al.[8] found a possible Northern European warming response to the AMV during winter, which they did not discuss in detail. Their study used two different GCMs (GFDL CM2.1 and NCAR CESM1) and restored North Atlantic SST to observe anomalies associated with AMV variability. In addition, the oscillatory relationship between the time-integrated NAO and the AMOC is discussed by Omrani et al.[9] and supports the strong temperature impact found during winter. Omrani et al.[9] argue that during and just after an AMV+ event, when sea ice melts in the Arctic peaks, Eurasia is warmer due to poleward oceanic heat transport. They found that the warming response also includes the Baltic Sea area. Using the regional atmospheric forcing, the associated regional SAT response to AMV/BMV variability also supports this warming response (Supplementary Figs. 5 and 6). We find the strongest impact in the Baltic Sea in regions where sea ice is formed. Further analysis

linked decreasing sea ice to positive BMV phases (not shown) and reducing the ice-snow albedo in regions where sea ice is formed (Supplementary Fig. 7). In fact, reduced precipitation during winter over Northern Europe was related to positive AMV+ phases[7] leading to less snowfall, also supporting the reduction of the ice-snow albedo over the Baltic Sea. Hence, there may be a link between the BMV signal and the yearly sea ice cover in the Baltic Sea, supporting earlier hints of changing sea ice cover[22].

Summarizing, our results suggest that the ocean is the main source of inertia that maintains the anomalous warm SST in the North Atlantic through increased northward oceanic heat transport, influencing the North Atlantic and the Baltic Sea. This warming is likely amplified by a smaller ice/snow albedo, causing even stronger warming due to decreasing sea ice cover in the Baltic Sea.

In our study, we discriminate between the AMV and the BMV. The difference in seasonal dynamics in the Baltic Sea becomes apparent when regressing the AMV signal onto the Baltic Sea SST (Fig. 3). The AMV projects a weak warming response for the Baltic Sea. In contrast, the BMV that emerges from the LFCA analysis of the Baltic Sea SST signal shows a three times stronger response. This is likely related to seasonal dynamics within the Baltic Sea that cannot be captured by regressing the SST onto the AMV signal. The strong seasonality of the Baltic Sea also influences the low frequency to total variance ratio (around 40%) of the BMV, which is relatively low compared to the AMV (78%). Analyzing the seasonal SST response associated with the AMV (Supplementary Figure 1) and the traditional AMV definition by Trenberth and Shea (Supplementary Fig. 2) shows that all indices show the strongest impact during winter but have little to no explained variance.

We find that using LFCA allows for analyzing the seasonal response of a regional climate system associated with AMV variability. In that way, we have been able to show that the winter season in the Baltic Sea and the SAT in Northern Europe are likely under the strong influence of the AMV, which has not been discussed in detail. Further, we find that the seasonal response within the Baltic Sea is strongly heterogonous and non-linear, as the spring season is not influenced at all. We thus propose to consider multi-decadal variations of Baltic Sea SST linked to but also partly autonomous from the AMV. While we focus on the effects of the AMV on the Baltic Sea, many other regional climate systems could be analyzed using LFCA without exclusively focusing on the AMV.

In summary, multidecadal fluctuations in the Baltic Sea, which are very similar to the AMV and for which we introduce the term BMV, have the greatest influence on SST in winter. The BMV turns out to be better suited for analyzing the teleconnection with the North Atlantic and the Baltic Sea than the original AMV signal.

METHODS

Regional ocean model
This work considers 1900–2008 using a historical climate simulation[27]. The model used for this study is the Rossby Centre Ocean model (RCO) coupled with the Swedish Coastal and Ocean Biogeochemical Model (RCO-SCOBI)[29,30]. RCO is a Bryan-Cox-Semtner primitive equation ocean model with a free surface. An open boundary in the northern Kattegat limits the model domain. RCO uses a two-equation closure k-epsilon turbulence model. The ocean model is coupled with a Hibler-type multi-category sea ice model. The bathymetry is based on topography data by Seifert and Kayser[31]. The horizontal resolution of the model is 3.7 km. Further, RCO uses 83 vertical levels with a layer thickness of 3 m resulting in a maximum depth of 250 m. RCO is forced by High-Resolution atmospheric Forcing Fields (HiResAFF)[32]. A more detailed description of the atmospheric fields is given in[27]. A

detailed assessment of this simulation can be found in[27]. Furthermore, Kniebusch et al.[23] focused on the SST signal in RCO. They discovered that RCO slightly underestimates the SST but is still within the standard deviation of the observations.

Extended reconstructed SST (ERSST)
For the North Atlantic, we use observed SST from 1900 to 2008. The ERSST dataset has a $2° \times 2°$ horizontal grid resolution and covers the period 1854 to the present (Huang et al., 2017). It uses COADS 3.0, which combines SST from Argo floats (above 5 m), Hadley Centre Ice-SST version 2 (HadISST2) ice concentration (1854–2015), and NCEP ice concentration (2016–present). Like[14], we decided to use the period 1900 to 2008 as the data gets more reliable after the 19th century.

ERA-20C
For the North Atlantic domain, we use atmospheric fields from ERA-20C, an atmospheric reanalysis from the 20th century covering the period 1900–2010[33]. ERA-20C was created as part of the ERA-CLIM project (see http://era-clim.eu) and is based on ECMWF's Integrated Forecast System.

It assimilates surface pressure and surface winds only and has a horizontal resolution of roughly 125 km (spectral truncation T159) and 91 vertical levels between the surface and 0.01 hPa. For the analysis, SLP, SAT, SST, and zonal winds at 700 hPa have been used.

Low-frequency component analysis
LFCA[26] allows for identifying modes of low-frequency variability. LFCA solves for linear combinations of EOFs that maximize the ratio of low frequency to the total variance. In other words, LFCA maximizes the fraction of a signal defined as low frequency. For a detailed description, the reader is referred to the original work[26]. However, in the following, a short introduction to LFCA is given based on the description in Wills et al.[26].

LFCA starts with a conventional principal component analysis (PCA) that identifies spatial patterns explaining large parts of the variance in the data. For the study, the data is converted to an $n \times p$ spatio-temporal matrix $\mathbf{X}$ with zero time mean.

The EOF can be computed by solving for the eigenvectors $\boldsymbol{a}_k$ of the sample covariance matrix

$$\mathbf{C} = \frac{1}{(n-1)} \mathbf{X}^T \mathbf{X}, \tag{1}$$

such that $\boldsymbol{C} \boldsymbol{a}_k = \sigma_k^2 \boldsymbol{a}_k$.

The EOFs are normalized ($\|\boldsymbol{a}_k\| = 1$), so that the eigenvalue σ_k^2 gives the variance associated with the kth EOF. The kth principal component (PC) is then defined by projecting the kth EOF onto the data matrix $\mathbf{X}$

$$PC_k = \sigma_k^{-1} \mathbf{X} \mathbf{a_k}. \tag{2}$$

For the LFCA, a linear Lanczos lowpass filter (L) with a cutoff frequency T^{-1} is used[34], which allows obtaining a lowpass filtered data matrix $\tilde{\mathbf{X}} = L(T)\mathbf{X}$. In our analysis, we define T to be 10 years.

The projection of $\tilde{\mathbf{X}}$ onto the kth EOF results in a lowpass filtered kth principal component

$$\overline{\mathbf{PC}} = \sigma_k^{-1} \tilde{\mathbf{X}} \mathbf{a_k}. \tag{3}$$

Then, LFCA searches for linear combinations $\mathbf{u}_k$ of the first N EOFs $\mathbf{a_1}, ..., \mathbf{a_N}$,

$$\mathbf{u_k} = \begin{bmatrix} \dfrac{\mathbf{a_1}}{\sigma_1} & \dfrac{\mathbf{a_2}}{\sigma_2} & ... & \dfrac{\mathbf{a_N}}{\sigma_N} \end{bmatrix} \mathbf{e_k} \tag{4}$$

where the square brackets indicate a $p \times N$ matrix. The coefficients $\mathbf{e_k}/\sigma_k$ shall be chosen in such a way that the ratio r_k of low-frequency to total variance is maximized. The ratio is defined as

$$r_k = \frac{\left(\widetilde{Xu_k}\right)^T \widetilde{Xu_k}}{\left(Xu_k\right)^T Xu_k} = \frac{u_k^T L^T C L u_k}{u_k^T C u_k}. \tag{5}$$

The coefficient vectors e_k are defined as normalized such that $||e_k|| = 1$. The normalization factors σ_k^{-1} then give the linear combinations u_k unit variance like the $\mathbf{a_k}$ have.

Using the equations above and the definition of a PC, it can be shown that the coefficient vectors $\mathbf{e_k}$ are eigenvectors of the covariance matrix

$$\mathbf{R_{ij}} = cov\left(\widetilde{PC_i}, \widetilde{PC_j}\right) \text{for i, } j\epsilon[1, N]. \tag{6}$$

R has N eigenvectors $\mathbf{Re_k} = r_k\mathbf{e_k}$, and they are sorted by the magnitude of the eigenvalues r_k.

The kth so-called LFC can be computed by projecting the unfiltered data onto the linear combination vectors u_k.

$$LFC_k = Xu_k \tag{7}$$

the associated so-called LFP can be computed by the regression of the unfiltered data onto the kth LFC,

$$\mathbf{LFP}_k = \mathbf{X^T} LFC_k \tag{8}$$

DATA AVAILABILITY

CODE AVAILABILITY

REFERENCES

1. Hasselmann, K. Stochastic climate models Part I. Theory. *Tellus* **28**, 473–485 (1976).
2. Trenberth, K. E. and Shea, D. J. Atlantic hurricanes and natural variability in 2005. *Geophys. Res. Lett.* https://doi.org/10.1029/2006GL026894 (2006).
3. Zhang, R. et al. A review of the role of the Atlantic meridional overturning circulation in Atlantic Multidecadal Variability and associated climate impacts. *Rev. Geophys.* **57**, 316–375 (2019).
4. Clement, A. et al. The Atlantic Multidecadal Oscillation without a role for ocean circulation. *Science* **350**, 320–324 (2015).
5. Mann, M. E., Steinman, B. A., Brouillette, D. J. & Miller, S. K. Multidecadal climate oscillations during the past millennium driven by volcanic forcing. *Science* **371**, 1014–1019 (2021).
6. Sutton, R. T. & Dong, B. Atlantic Ocean influence on a shift in European climate in the 1990s. *Nat. Geosci.* **5**, 788–792 (2012).
7. Börgel, F. et al. Atlantic Multidecadal Variability and the implications for North European precipitation. *Environ. Res. Lett.* **17**, 044040 (2022).
8. Ruprich-Robert, Y. et al. Assessing the climate impacts of the observed Atlantic Multidecadal Variability using the GFDL CM2.1 and NCAR CESM1 global coupled models. *J. Clim.* **30**, 2785–2810 (2017).
9. Omrani, N.-E. et al. Coupled stratosphere-troposphere-Atlantic multidecadal oscillation and its importance for near-future climate projection. *Npj Clim. Atmos. Sci.* **5**, 59 (2022).
10. Borchert, L. F. et al. Decadal predictions of the probability of occurrence for warm summer temperature extremes. *Geophys. Res. Lett.* **46**, 14042–14051 (2019).
11. Hurrell, J. W. Decadal trends in the North Atlantic Oscillation: regional temperatures and precipitation. *Science* **269**, 676–679 (1995).
12. Yamamoto, A. & Palter, J. B. The absence of an Atlantic imprint on the multidecadal variability of wintertime European temperature. *Nat. Commun.* **7**, 1–8 (2016).
13. Sun, C., Li, J. & Jin, F.-F. A delayed oscillator model for the quasi-periodic multidecadal variability of the NAO. *Clim. Dyn.* **45**, 2083–2099 (2015).
14. Wills, R. C. J., Armour, K. C., Battisti, D. S. & Hartmann, D. L. Ocean-atmosphere dynamical coupling fundamental to the Atlantic multidecadal oscillation. *J. Clim.* **32**, 251–272 (2019).
15. Börgel, F., Frauen, C., Neumann, T. & Markus Meier, H. E. The Atlantic Multidecadal Oscillation controls the impact of the North Atlantic Oscillation on North European climate. *Environ. Res. Lett.* **15**, 104025 (2020).
16. Wills, R. C. J., Armour, K. C., Battisti, D. S. & Hartmann, D. L. Ocean–atmosphere dynamical coupling fundamental to the Atlantic Multidecadal Oscillation. *J. Clim.* **32**, 251–272 (2019).
17. Sutton, R. T. et al. Atlantic Multidecadal Variability and the U.K. ACSIS program. *Bull. Am. Meteorol. Soc.* **99**, 415–425 (2018).
18. Enfield, D. B., Mestas-Nuñez, A. M. & Trimble, P. J. The Atlantic multidecadal oscillation and its relation to rainfall and river flows in the continental U.S. *Geophys. Res. Lett.* **28**, 2077–2080 (2001).
19. Frankcombe, L. M., von der Heydt, A. & Dijkstra, H. A. North Atlantic multidecadal climate variability: an investigation of dominant time scales and processes. *J. Clim.* **23**, 3626–3638 (2010).
20. Zanchettin, D. et al. Background conditions influence the decadal climate response to strong volcanic eruptions. *J. Geophys. Res. Atmos.* **118**, 4090–4106 (2013).
21. Casanueva, A., Rodríguez-Puebla, C., Frías, M. D. & González-Reviriego, N. Variability of extreme precipitation over Europe and its relationships with teleconnection patterns. *Hydrol. Earth Syst. Sci.* **18**, 709–725 (2014).
22. Börgel, F., Frauen, C., Neumann, T., Schimanke, S. & Meier, H. E. M. Impact of the Atlantic multidecadal oscillation on baltic sea variability. *Geophys. Res. Lett.* **45**, 9880–9888 (2018).
23. Kniebusch, M., Meier, H. E. M., Neumann, T. & Börgel, F. Temperature variability of the Baltic Sea since 1850 and attribution to atmospheric forcing variables. *J. Geophys. Res. Oceans* **124**, 4168–4187 (2019).
24. Hurrell, J. W., Kushnir, Y., Ottersen, G. & Visbeck, M. An Overview of the North Atlantic Oscillation, in *The North Atlantic Oscillation: Climatic Significance and Environmental Impact*, (American Geophysical Union (AGU), 2003) 1–35. https://doi.org/10.1029/134GM01.
25. Ruggieri, P. et al. Atlantic Multidecadal Variability and North Atlantic jet: a multimodel view from the decadal climate prediction project. *J. Clim.* **34**, 347–360 (2021).
26. Wills, R. C., Schneider, T., Wallace, J. M., Battisti, D. S. & Hartmann, D. L. Disentangling global warming, multidecadal variability, and El Niño in pacific temperatures. *Geophys. Res. Lett.* **45**, 2487–2496 (2018).
27. Meier, H. E. M. et al. Disentangling the impact of nutrient load and climate changes on Baltic Sea hypoxia and eutrophication since 1850. *Clim. Dyn.* **53**, 1145–1166 (2019).
28. Oldenburg, D., Wills, R. C. J., Armour, K. C., Thompson, L. & Jackson, L. C. Mechanisms of low-frequency variability in north Atlantic ocean heat transport and AMOC. *J. Clim.* **34**, 4733–4755 (2021).
29. Eilola, K., Meier, H. E. M. & Almroth, E. On the dynamics of oxygen, phosphorus and cyanobacteria in the Baltic Sea; a model study. *J. Mar. Syst.* **75**, 163–184 (2009).
30. Meier, H. E. M., Döscher, R. & Faxén, T. A multiprocessor coupled ice-ocean model for the Baltic Sea: application to salt inflow. *J. Geophys. Res. Oceans* https://doi.org/10.1029/2000JC000521 (2003).
31. Seifert, T. & Kayser, B. A high resolution spherical grid topography of the Baltic Sea, *Meereswiss Ber Warn.* vol. 9, (Institut fur Ostseeforschung, 1995).
32. Schenk, F. & Zorita, E. Reconstruction of high resolution atmospheric fields for Northern Europe using analog-upscaling. *Clim. Past Discuss.* **8**, 819–868 (2012).
33. Poli, P. et al. ERA-20C: an atmospheric reanalysis of the twentieth century. *J. Clim.* **29**, 4083–4097 (2016). Jun.
34. Duchon, C. E. Lanczos filtering in one and two dimensions. *J. Appl. Meteorol. 1962–1982* **18**, 1016–1022 (1979).

AUTHOR CONTRIBUTIONS

F.B. designed the research, analyzed the model results, and wrote the paper's text with the help of all co-authors. H.E.M.M. performed the model simulation.

COMPETING INTERESTS

The author declares no competing interests.

ADDITIONAL INFORMATION

Supplementary information The online version contains supplementary material available at https://doi.org/10.1038/s41612-023-00373-8.

Correspondence and requests for materials should be addressed to Florian Börgel.

Reprints and permission information is available at http://www.nature.com/reprints

Publisher's note Springer Nature remains neutral with regard to jurisdictional claims in published maps and institutional affiliations.